

# Energy Loss and Microturbulence under Multipulse ECR Plasma Heating at the L-2M Stellarator

G. M. Batanov<sup>a,\*</sup>, V. D. Borzosekov<sup>a,\*\*</sup>, D. G. Vasilkov<sup>a, b</sup>, S. E. Grebenshchikov<sup>a</sup>,  
L. V. Kolik<sup>a</sup>, E. M. Konchekov<sup>a</sup>, A. A. Letunov<sup>a</sup>, A. E. Petrov<sup>a</sup>,  
V. D. Stepakhin<sup>a</sup>, N. K. Kharchev<sup>a</sup>, and A. A. Kharchevskii<sup>a</sup>

<sup>a</sup> Prokhorov General Physics Institute of the Russian Academy of Sciences, Moscow, 119991 Russia

<sup>b</sup> Bauman Moscow State Technical University, Moscow, 105005 Russia

\*e-mail: batanov@fpl.gpi.ru

\*\*e-mail: borzosekov@fpl.gpi.ru

Received January 14, 2019; revised March 13, 2019; accepted March 25, 2019

**Abstract**—In experiments on multipulse on-axis electron cyclotron resonance heating (ECRH) of plasma by a series of microwave pulses at the L-2M stellarator, several phases of plasma energy loss were observed: the short stage of low-energy loss, the stage of rapid increase in energy loss, the quasi-steady stage, and the relaxation stage between the heating pulses. In the stage of rapid increase in energy loss, the energy loss power is two or more times higher than that in the relaxation stage at the same energy of the plasma column. Short-wavelength plasma density fluctuations were measured using both the ordinary and extraordinary microwave collective scattering technique. It is found that, in the quasi-steady stage, the amplitude of density fluctuations is much lower than that in the preceding heating stages. The fluctuation amplitude lowers just after the restructuring of the density profile and establishment of a steady-state hollow density profile due to the density pump-out effect. The amplitude of large-scale density fluctuations at the plasma periphery recorded by a Doppler reflectometer remains unchanged during the ECRH pulses and in the time intervals between them. However, when the stage of rapid increase in energy loss begins, the shape of the density fluctuation spectrum changes significantly. The initially narrow spectrum with one peak near the zero frequency broadens, the amplitude of the central peak decreases, and two additional peaks at frequencies of 0.7 and  $-0.7$  MHz appear.

DOI: 10.1134/S1063780X19080014

## 1. INTRODUCTION

The multipulse mode of electron cyclotron resonance heating (ECRH) of plasma by a train of microwave pulses is of interest because it allows one to study various transport processes and their effect on the time evolution of the plasma parameters, such as the temperature and density profiles of charged particles and the characteristics of microturbulences of different scales and nature. In the experiments carried out at the L-2M stellarator [1], it was shown that, after the beginning of the ECRH pulse, there is a time interval during which the energy loss power varies only slightly. At the end of this time interval, the loss power begins to rapidly increase up to the value at which the loss power becomes equal to the ECRH power. If the ECRH power  $P_{\text{ECRH}}$  increases twice (from 0.2 to 0.4 MW), then the time interval in which the loss power varies weakly nearly halves. The goal of this work was to find out whether changes in the loss power correlate with time variations in the density and temperature profiles, as well as with changes in the ampli-

tude and spectral composition of turbulent fluctuations of the plasma density.

## 2. EXPERIMENTAL CONDITIONS AND DIAGNOSTIC TECHNIQUES

The experiments on multipulse on-axis ECRH of plasma by a train of microwave pulses were carried out in the main magnetic configuration of the L-2M stellarator (Fig. 1). Multipulse ECRH was switched on at 48 ms, when the gyroresonance at a frequency of  $f = 75$  GHz was located at a major radius of  $R_0 = 97$  cm. At 54 ms, the magnetic axis and gyroresonance are located at the axis of the vacuum chamber ( $R_0 = 100$  cm), while at 60 ms, the gyroresonance location again shifts to  $R_0 = 98$  cm. In these experiments, the ECRH power  $P_{\text{ECRH}}$  in each microwave pulse of the train was 0.4 MW, while the pulse duration  $\tau_p$  was either 2.2 ms (Figs. 1a–1d) or 3.7 ms (Figs. 1e–1h). There were different time intervals  $\tau_{\text{br}}$  (pauses) between the pulses: 2.3 ms, 4.3 ms (Figs. 1e–1h), and

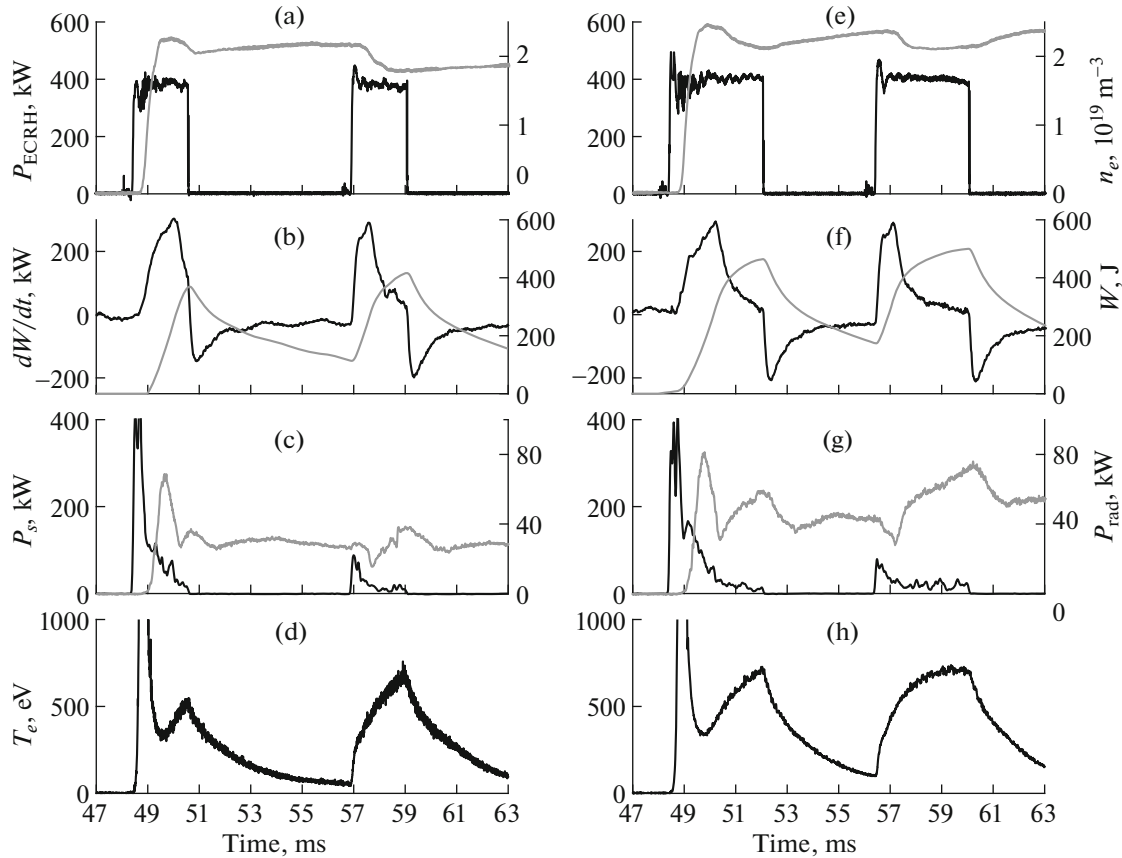


**Fig. 1.** Time evolution of the plasma macroparameters in the L-2M stellarator during multipulse ECRH in (a–d) shot no. 21354 (ECRH pulse duration  $\tau_p = 2.2$  ms, duration of pauses between pulses  $\tau_{br} = 6.3$  ms) and (e–h) shot no. 21375 ( $\tau_p = 3.7$  ms,  $\tau_{br} = 4.3$  ms): (a, e) ECRH power  $P_{\text{ECRH}}$  (black curve) and the average electron density  $n_e$  (grey curve), (b, f) diamagnetic response  $dW/dt$  (black curve) and plasma energy content  $W$  (grey curve), (c, g) ECRH power unabsorbed in plasma  $P_s$  (black curve) and radiative loss power  $P_{\text{rad}}$  (grey curve), and (h) electron temperature at the plasma column axis. In all plots with two ordinates, the left and right ordinates correspond to the black and grey curves, respectively.

6.3 ms (Figs. 1a–1d). The plasma density measured with a 2-mm interferometer along the vertical chord of the plasma column within one series of pulses was usually in the range of  $(1.9\text{--}2.1) \times 10^{13} \text{ cm}^{-3}$ . The electron temperature in the heating region obtained from measurements of the electron cyclotron radiation at the second harmonic of the electron gyrofrequency (74 GHz) [2] and plasma soft X-ray spectra [3] reached 0.7 keV. The time evolution of the plasma density profile in one of the heating modes was measured with an HCN interferometer operating at the wavelength  $\lambda = 337 \mu\text{m}$  [4].

Plasma density fluctuations were measured using collective scattering of the heating gyrotron radiation. The following methods were used: backscattering from short-wavelength fluctuations ( $k = 30 \text{ cm}^{-1}$ ), small-angle scattering from long-wavelength fluctuations ( $k = 1 \text{ cm}^{-1}$ ), and Bragg side scattering from short-wavelength fluctuations ( $k = 20 \text{ cm}^{-1}$ ) in the ECRH region [5–7]. Long-wavelength fluctuations of the

plasma density ( $k = 2 \text{ cm}^{-1}$ ) at the plasma periphery were measured using backscattering of the Doppler reflectometer radiation (37.5 GHz) [8]. The incidence angle of the ordinary (O) reflectometer wave relative to the normal to the boundary magnetic surface was  $16^\circ$ . This made it possible to measure density fluctuations at the edge of the plasma column (at  $r/a = 0.8\text{--}0.9$ ), where the density reached  $1.7 \times 10^{13} \text{ cm}^{-3}$ .

We also measured unabsorbed and reemitted microwave radiation with wavelengths of  $\lambda \leq 4 \text{ mm}$  by means of a microwave detector with an absorbing collimator installed in the stellarator port located in the poloidal cross section of the torus shifted by  $90^\circ$  with respect to the cross section in which gyrotron radiation was launched.

### 3. MEASUREMENT RESULTS AND DISCUSSION

When determining the energy loss power from the plasma column, we take into account that, in the time

intervals between the ECRH pulses, the plasma diamagnetic response  $dW/dt$  (time derivative of the plasma energy content) is related to the total loss power  $P_{\text{los}}$  (including the radiative loss power  $P_{\text{rad}}$ ) as

$$P_{\text{los}} = -dW/dt. \quad (1)$$

The fact that, 5–6 ms after the end of the ECRH pulse,  $P_{\text{rad}} \equiv -dW/dt$ , the average plasma density being unchanged, can be used to absolutely calibrate the radiative loss signal.

Since the plasma column forms in the first pulse of the train and the average plasma density remains unchanged for about 10 ms (during and even after the train), the diamagnetic response  $dW/dt$  in the second and subsequent pulses is equal to the power spent on the increase in the charged particle energy, i.e., it is equal to the gyrotron radiation power  $P_0$  minus the unabsorbed heating power  $P_s$  (the microwave power escaping through the ports of the vacuum chamber), the radiative loss power, and the heat loss power  $P_{2\text{los}}$  (the heat flux onto the vacuum chamber wall),

$$\begin{aligned} dW/dt &= P_0 - P_s - P_{\text{rad}} - P_{2\text{los}}, \\ \text{or } P_{2\text{los}} &= P_0 - dW/dt - P_{\text{rad}} - P_s. \end{aligned} \quad (2)$$

Figure 1 shows time dependences of the plasma macroparameters in two experimental regimes. It can be seen that the average plasma density varies only slightly during the train of microwave pulses, remaining at a level of about  $2 \times 10^{13} \text{ cm}^{-3}$ . In the time intervals between the heating pulses, both the plasma energy  $W$  and the central temperature  $T_e(0)$  decrease. The longer the time interval  $\tau_{\text{br}}$  between the heating pulses, the stronger the decrease. The signals from the detector measuring the unabsorbed microwave power  $P_s$  (the power escaping through the ports of the vacuum chamber) are also shown in Fig. 1. This power can be estimated from the spike at the leading edge of the first pulse in the train, assuming that the amplitude of this spike is proportional to the total power  $P_0$  introduced in the chamber. By the end of the first pulse, the unabsorbed power  $P_s$  comprises approximately 20% of the total input power, whereas by the middle of the second ECRH pulse, it decreases to 10%. However, as the time interval  $\tau_{\text{br}}$  between the pulses rises to 4.3 ms, the power  $P_s$  at the leading edges of the second and subsequent pulses increases to more than 25%. Apparently, this is related to the drop in the electron temperature and the corresponding drop in the absorption coefficient during one pass of the microwave beam through the gyroresonance region.

After these preliminary remarks, let us now consider the time evolution of the heat loss power  $P_{2\text{los}}$ . We chronologically denominate the characteristic time intervals in the order of their occurrence after the beginning of the ECRH pulse (Fig. 2) as follows: (I)

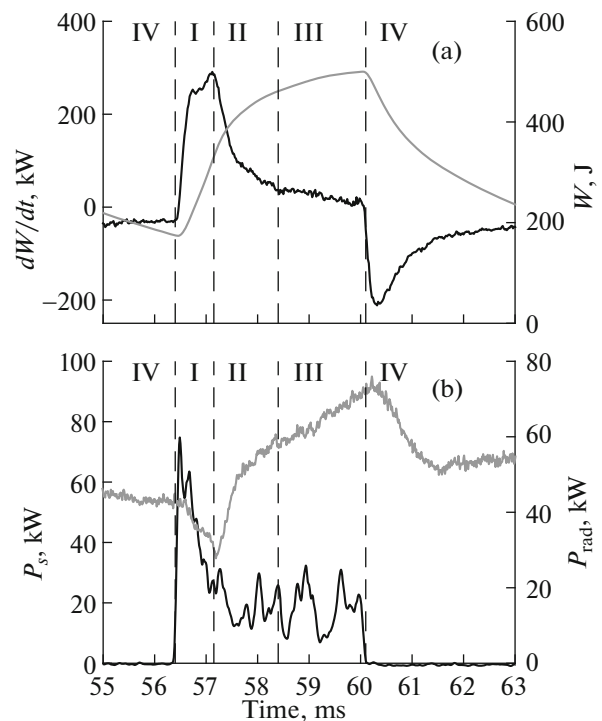


**Fig. 2.** Characteristic stages of the plasma energy loss in the L-2M stellarator during multipulse ECRH, exemplified by the second heating pulse in shot no. 21375: (a) diamagnetic response  $dW/dt$  (black curve) and plasma energy content  $W$  (grey curve) and (b) ECRH power unabsorbed in plasma  $P_s$  (black curve) and radiative loss power  $P_{\text{rad}}$  (grey curve). In all plots with two ordinates, the left and right ordinates correspond to the black and grey curves, respectively, and the vertical thin dashed lines show the boundaries of the characteristic stages.

the stage of low energy loss; (II) the stage of rapid increase in energy loss; (III) the quasi-stationary stage; and (IV) the relaxation stage, which lasts from the end of one ECRH pulse up to the beginning of the next one. These stages are repeated from pulse to pulse during the entire multipulse discharge. They were observed in all discharges with multipulse ECRH of the L-2M plasma at the heating powers, heating pulse durations, and interpulse pauses used in these experiments.

Further, we will focus on the time evolution of the plasma parameters during the second ECRH pulse, because, during a train of pulses, the gyroresonance region shifts in such a way that, in the second heating pulse, it is located close to the axis of the vacuum chamber ( $R_0 = 100 \text{ cm}$ ). Figure 2 shows time dependences of the diamagnetic response  $dW/dt$ , radiative loss power  $P_{\text{rad}}$ , and unabsorbed ECRH power  $P_s$  during the second heating pulse. In stage I, after the beginning of heating, the rise time of the  $dW/dt$  signal is determined by the response time of the stainless-steel chamber walls, which is 170  $\mu\text{s}$ . During the next 0.3 ms, the  $dW/dt$  signal varies only slightly. This

means that the energy loss power  $P_{2\text{los}}$  varies slightly, because  $P_{\text{rad}}$  and  $P_s$  are small and vary weakly during this time interval. According to formula (2), the energy loss power in stage I is  $P_{2\text{los}} = 60$  kW.

In stage II, the diamagnetic response  $dW/dt$  drops rapidly during 0.3–0.5 ms and then continues to drop more slowly, so that, at a pulse duration of 3.7 ms, it almost vanishes ( $dW/dt \approx 0$ ) by the end of stage III, which means that the heating power becomes equal to the loss power. The fast increase in the energy loss is due to an increase in the heat loss power, because, as is seen in Fig. 2, the radiative loss and the unabsorbed power loss through the ports of the vacuum chamber comprise a small fraction of the ECRH power. The transition to the “degraded” confinement mode similar to the transition from stage I to stage II was observed in the early experiments of ECRH of tokamak plasmas, e.g. at the T-10 tokamak [9], as well as at the ASDEX tokamak after the beginning of neutral beam injection experiments [10]. In both cases, it was shown that the duration of stage I with a low-energy loss can be increased by enhancing gas puffing.

It is natural to assume that the transport processes are different in the presence and absence of ECRH. It would be interesting to compare the power losses in these two stages at equal plasma energies. Such a comparison can be made for shot no. 21375, in which the plasma energy is  $W = 0.4$  kJ in both stage II (during the ECRH pulse) and stage IV (relaxation stage) (Fig. 2). For the times at which this plasma energy is achieved, we have  $dW/dt(\text{II}) = 115$  kW and  $dW/dt(\text{IV}) = -155$  kW. According to formulas (1) and (2), the corresponding heat loss powers are

$$\begin{aligned} P_{2\text{los}}(\text{II}) &= P_0 - dW/dt - P_{\text{rad}} - P_s \\ &= 400 - 115 - 55 - 15 = 215 \text{ kW}, \\ P_{2\text{los}}(\text{IV}) &= |dW/dt| - P_{\text{rad}} = 155 - 55 = 100 \text{ kW}. \end{aligned}$$

We see that the heat loss power in heating stage II is least two times higher than in relaxation stage IV. Now, before presenting results of measurement of turbulent plasma density fluctuations, it is necessary to make the following remark. Since the mean free path of electrons in the hot stellarator plasma is much longer than the torus circumference, the results of measurements of the electron temperature and diamagnetic signal are averaged over the circumference of the torus. At the same time, measurements of density fluctuations are local and, as was noted in [11], they are not synchronous in different poloidal cross sections. Therefore, the time evolution of turbulent density fluctuations can be compared with the time evolution of the electron temperature and heat loss power only qualitatively.

Let us briefly dwell on the question concerning the effect of the durations of the heating pulses  $\tau_p$  and pauses between them  $\tau_{\text{br}}$  on the plasma parameters

under study. Changing the durations of the ECRH pulses and time intervals between them, we change the initial conditions for the microwave beam–plasma interaction. In this case, the following factors change: the initial electron temperature and the radial profiles of the density and temperature. At the same time, it follows from the 2-mm-interferometer signals (Fig. 1) that the average plasma density is preserved. At the doubled pulse duration  $\tau_p$ , the radiative loss power at the end of stage III increases only slightly (approximately by one-third). The threefold increase in the pause  $\tau_{\text{br}}$  between the heating pulses increases the duration of stage I in the diamagnetic response  $dW/dt$  by 100–150  $\mu\text{s}$ .

Figure 3 shows the time dependence of the squared amplitude of density fluctuations  $n_e^2$  obtained using the radiation scattering technique described in [12]. The figure gives an idea of the time evolution of the density fluctuation level. The results of backscattering measurements characterize the fluctuation level averaged over the microwave beam path from the boundary magnetic surface to the gyroresonance region, while the results of small-angle scattering measurements are averaged over the entire chord of the plasma column. The results of Bragg side scattering measurements characterize the time evolution of density fluctuations in the ECRH region.

All scattering diagnostics at the L-2M stellarator can be adjusted to receive either the ordinary (O) or extraordinary (X) microwave signal. This is very useful under ECRH conditions at the L-2M stellarator, in which the initially linearly polarized microwave radiation splits into the X and O components [13] and both these components are scattered from density fluctuations. In these experiments, in order to reveal differences in the time evolution of the X- and O-polarized microwaves, both X and O scattering signals were recorded. These signals actually differs substantially. The main difference is that, in ECRH stage II, the drop in the scattered radiation intensity and the transition to a certain quasi-steady level of fluctuations for the X-wave occur 1.5 ms earlier than those for the O-wave. Presumably, this difference in the X and O scattering signals is due to the electron cyclotron resonance absorption of X-waves. In [14], it was shown that, in the magnetic configuration of the L-2M stellarator, under the ECRH conditions at an average plasma density of  $n_e = 2 \times 10^{13} \text{ cm}^{-3}$  and a hollow density profile, the X-polarized microwave beam can partially deviate into the lower half-plane of the torus. On the other hand, the refraction of the O-wave is weak: the refractive index of the O-wave is 0.77, and it experiences almost no electron cyclotron resonance absorption. Therefore, to analyze the time evolution of the density fluctuation level, it is reasonable to use the O scattering signal.

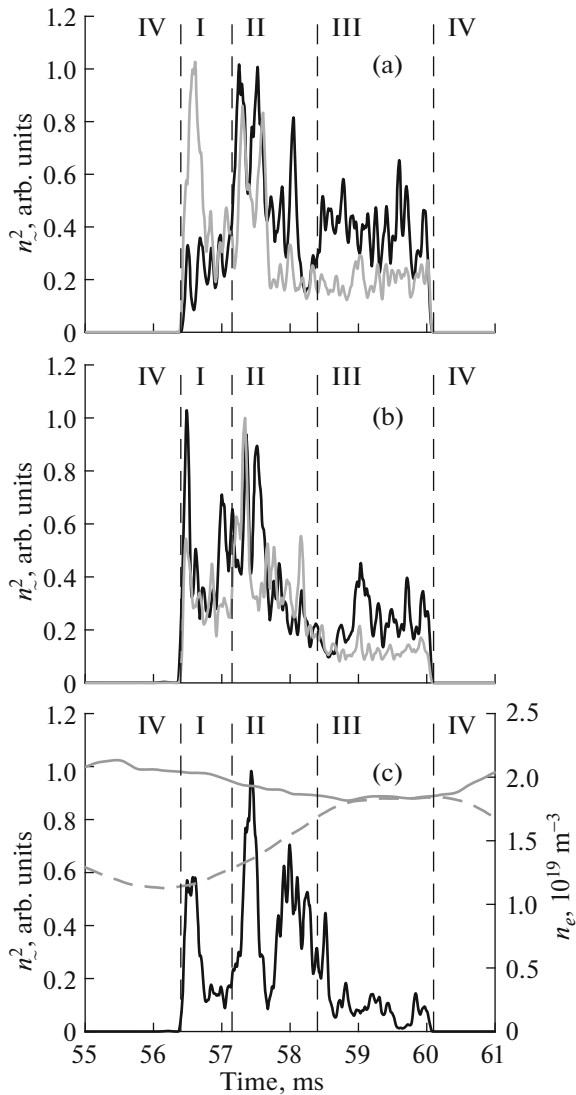


**Fig. 3.** Time evolution of the microturbulence intensity in shot no. 21375: (a) intensity of short-wavelength density fluctuations  $n_s^2$  measured using Bragg side scattering into the upper half-plane of the torus from the local region centered on the axis of the vacuum chamber (black curve) and from the region shifted by 2 cm outward from the chamber axis (grey curve), (b) intensity of short-wavelength density fluctuations  $n_s^2$  averaged over half of the central chord (black curve) and intensity of long-wavelength density fluctuations averaged over the entire length of the central chord (grey curve), and (c) intensity of short-wavelength density fluctuations  $n_s^2$  in the plasma core measured using Bragg side scattering into the lower half-plane of the torus (black curve, left ordinate) and plasma density  $n_e$  (right ordinate) measured by the laser interferometer along the central and peripheral chords (solid and dashed grey curves, respectively).

Using the results of all collective scattering diagnostics, it can be stated that, for all recorded fluctuation wavelengths and all observation regions, the time

dependences of the density fluctuation level are similar. First, in almost all shots, a short spike (0.2–0.3 ms) in the fluctuation intensity  $n_s^2$  is observed in ECRH stage I. This spike occurs simultaneously with the beginning of the growth of the electron temperature  $T_e$  in the gyroresonance region. Presumably, it is caused by a sharp perturbation of the plasma density in the narrow resonance region or by the parametric decay instability developing in this region [15]. Second, in ECRH stage II, the intensity of density fluctuations is a chain of high-amplitude flashes against a certain nonzero background. Third, by the time of completion of the density profile restructuring due to the density pump-out effect [16–21], a quasi-steady level of density fluctuations, lower than that in ECRH stage II, is established. An increase in the density fluctuation level during active restructuring of the density profile in the T-10 tokamak was reported in [22]. In that experiment, the fluctuation level also decreased after the completion of the density profile restructuring.

As can be seen from the above figures, the maximum level of short-wavelength density fluctuations corresponds to the highest rate of the density drop in the plasma core and the highest growth rate of the density at the plasma periphery. Thus, the high level of short-wavelength density fluctuations in the gyroresonance region is maintained during the entire ECRH pulse and is accompanied by the growth of the electron temperature and heat loss power, regardless of the initial temperature and the radial density profile. It should be noted, however, that there are some changes in the spectra of the short-wavelength density fluctuations (Fig. 4). During the transition from stage I to stage II, the fluctuation intensity increases in almost the entire frequency domain. According to the results from all diagnostics, the high frequency (HF) component ( $>1$  MHz) increases, but this spectral range contribute insignificantly to the total intensity of fluctuations. At the same time, the growth of low-frequency (LF) fluctuations ( $<300$  kHz) is not always clearly observed (see Figs. 4b, 4d). In ECRH stage III, the intensity of the LF component decreases substantially, while the HF component changes only slightly. In the framework of the model of self-organized criticality, a similar result can be obtained when the shear of the poloidal rotation velocity appears in the plasma (see, e.g., [23]).

In ECRH stages I and II, the intensity of fluctuations in the frequency range of up to 200–400 kHz is higher than in stage III. This was confirmed by all diagnostics, except for Bragg side scattering into the upper half-plane of the torus from a local region at the axis of the vacuum chamber. However, in ECRH stage III, the intensity of the HF component ( $>800$  kHz) is higher, which is most clearly pronounced in the fluctuation signal from in the above-mentioned local region (Fig. 4a). We note, however,

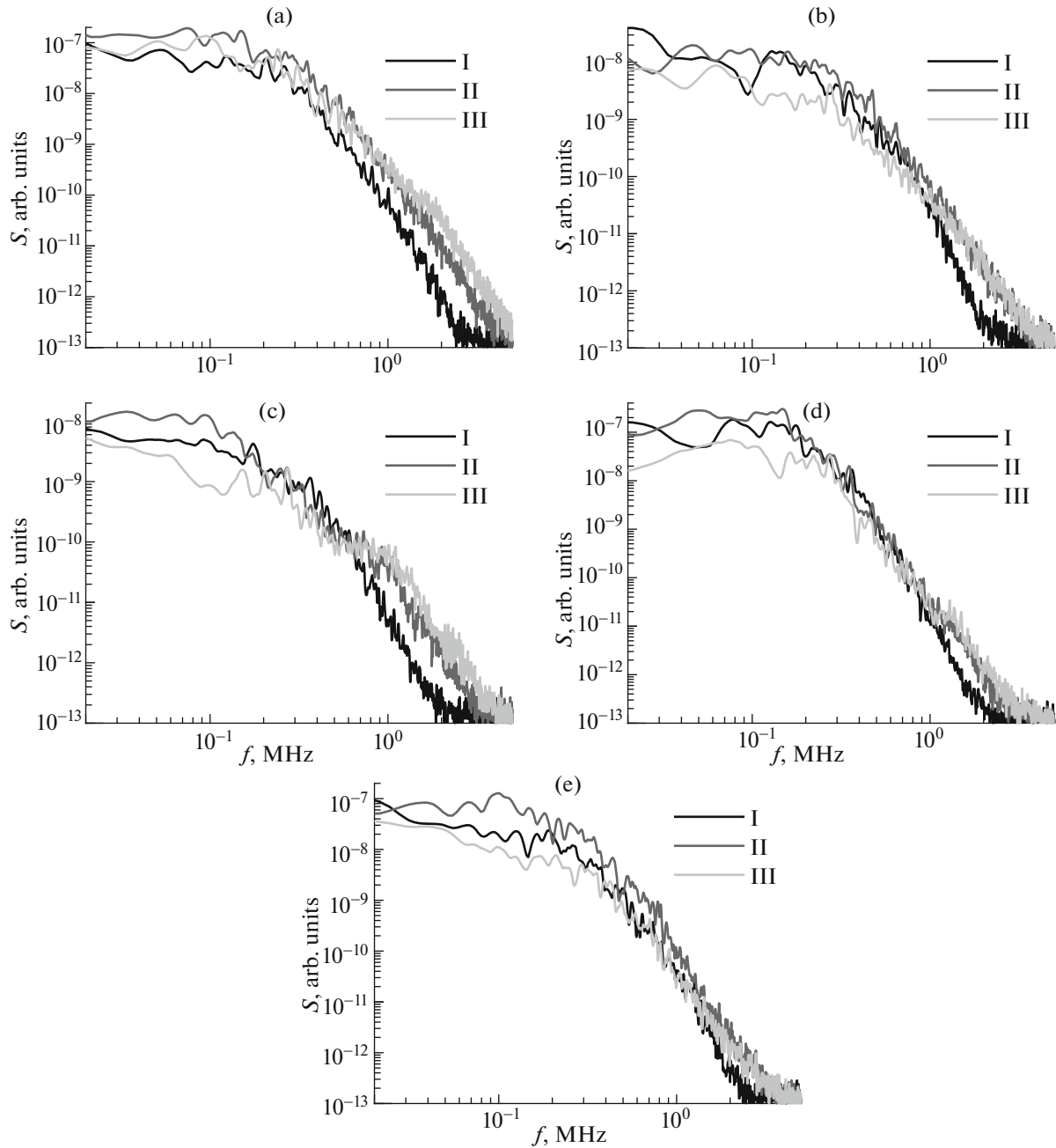


**Fig. 4.** Time evolution of the microturbulence spectra: (a) short-wavelength fluctuations in the local region centered on the axis of the vacuum chamber measured using Bragg side scattering into the upper half-plane of the torus, (b) short-wavelength fluctuations in the region shifted by 2 cm outward from the chamber axis, (c) short-wavelength fluctuations averaged over half of the central chord, (d) long-wavelength fluctuations averaged over the entire length of the central chord, and (e) short-wavelength fluctuations in the ECRH region measured using Bragg side scattering into the lower half-plane of the torus. In all plots, the black, dark grey, and light grey curves correspond to the spectra measured in ECRH stages I, II, and III, respectively.

that this spectral range makes almost no contribution to the total intensity of fluctuations.

The Doppler reflectometry of density fluctuations at the periphery of the plasma column shows that the fluctuation level remains almost unchanged both during ECRH pulses and between them, except for

ECRH stage III in the second pulse (Fig. 5). In this time interval, a decrease in the fluctuation level is observed, but it is not so strong as that recorded by the other scattering diagnostics measuring density fluctuations in the axial region of the plasma column and integrally along the chords. However, the spectra



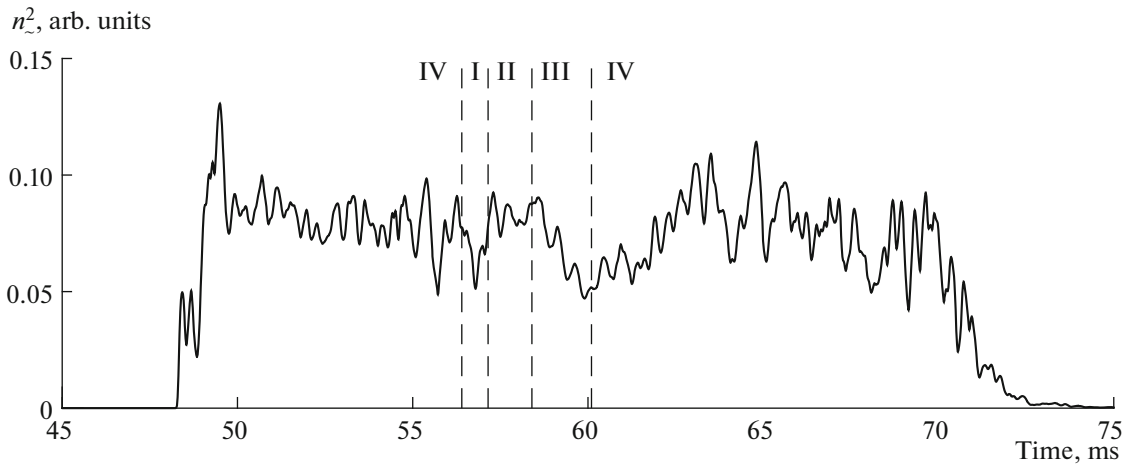


**Fig. 5.** Time evolution of the intensity of long-wavelength density fluctuations  $n^2$  at the edge of the plasma column.

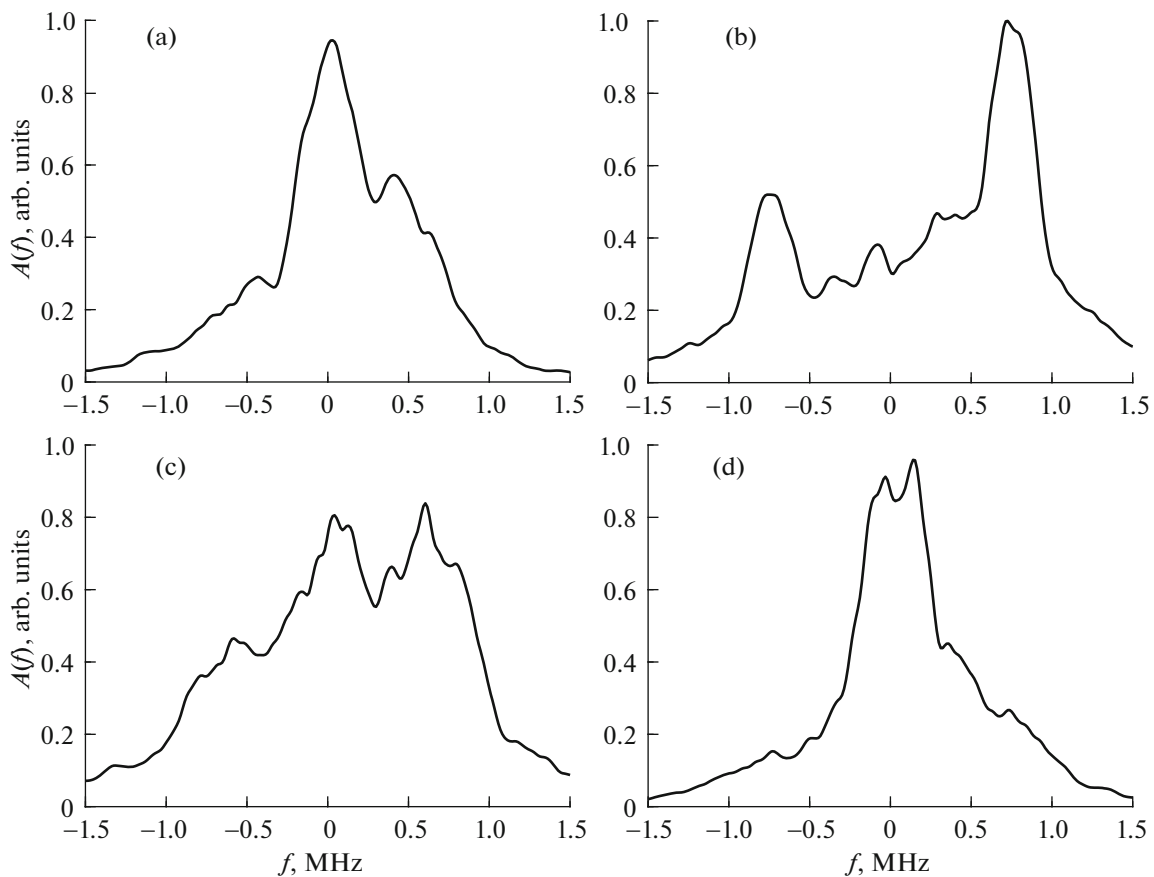


**Fig. 6.** Time evolution of the microturbulence spectra at the edge of the plasma column in different ECRH stages: (a) stage I, (b) stage II, (c) stage III and the first 2–3 ms after the beginning of stage IV, and (d) the rest of stage IV.

change substantially (Fig. 6). At the beginning of ECRH stage I, the spectrum has the shape of a Gaussian function centered at the zero frequency (Fig. 6a),

and such a shape survives during the entire stage I. The spectrum begins to change considerably at the beginning of ECRH stage II: the spectrum broadens appreciably

ciably and acquires a double-humped shape with a strongly suppressed central peak and two peaks near 0.7 and  $-0.7$  MHz,<sup>1</sup> the intensities of which differ twice (Fig. 6b). Such a shape is roughly preserved during both the entire ECRH stage III (except for a gradual increase in the amplitude of the central peak) (Fig. 6c) and 2–3 ms in the beginning of ECRH stage IV. After this, the spectrum again acquires the shape with a peak near the zero frequency. Comparing the time evolutions of the loss power and the fluctuation spectra recorded by the reflectometer, we see that the narrow-band spectra characterize fluctuations in the plasma with a low energy content and low temperature. Preservation of wide-band fluctuation spectra after the end of the ECRH pulse (stage IV) corresponds to the prolonged relaxation of the radial density profile after the heating is switched off. It is easy to see that, at the beginning of ECRH stage IV, the loss power decreases much faster than the fluctuation spectrum changes (Fig. 2).

#### 4. CONCLUSIONS

The time evolution of the loss power and turbulent density fluctuations were studied in the L-2M experiments on the ECRH of plasma with the mean density of  $2 \times 10^{13} \text{ cm}^{-3}$  by a train of microwave pulses with a power of 0.4 MW; ECRH pulse durations of 2.2 and 3.7 ms; and time intervals between the pulses of 2.3, 4.3, and 6.3 ms. In this way, the initial electron temperature and the initial radial profiles of the electron density and temperature in the subsequent ECRH pulses were varied.

It is shown that, at the beginning of the ECRH pulse, there is a short time interval of 0.5–0.7 ms (stage I) with a low energy loss. It is followed by stage II, during which the energy loss grows rapidly. At the end of this stage, the quasi-stationary mode of plasma confinement is established (stage III), in which the loss power is equal to the heating power. At the durations of ECRH pulses and pauses between them used in these experiments, the durations of stages I and II vary only slightly. It is found that, after ECRH is switched off (stage IV), the loss power is twice or more lower than that during the ECRH at equal energies of the plasma column.

Measurements of turbulent density fluctuations have shown that the maximum intensity of plasma density fluctuations in the plasma core is observed at the maximum rates of the density variation in the core and at the edge of the plasma column, rather than at the maximum energy loss from the plasma. Such behavior is similar to the results of T-10 experiments

[22], which demonstrated that the enhanced level of density fluctuations during the active rearrangement of the density profile corresponded to intense turbulent transport of particles, rather than of heat. At the edge of the plasma column, the level of long-wave fluctuations is maintained both during the heating pulses and in the time interval between them. After the beginning of the rapid increase in the energy loss, the spectrum of density fluctuations at the plasma periphery broadens appreciably and its shape changes from the distribution with a single peak near the zero frequency to the double-humped distribution, the peaks of which have different intensities and are shifted by 0.6–0.7 MHz relative to the zero frequency. During pauses between the ECRH pulses, the spectrum again becomes single-peaked with the maximum near the zero frequency, but only 2–3 ms after the end of the heating pulse.

#### FUNDING

This work was supported by the Russian Foundation for Basic Research, project no.18-02-00621.

#### REFERENCES

1. G. M. Batanov, M. S. Berezhetskiy, V. D. Borzosekov, S. E. Grebenshchikov, I. A. Grishina, V. A. Ivanov, N. K. Kharchev, A. A. Kharchevsky, Yu. V. Kholnov, L. V. Kolik, E. M. Konchekov, A. A. Letunov, V. P. Logvinenko, D. V. Malakhov, A. I. Meshcheryakov, et al., in *Proceedings of the 44th EPS Conference on Plasma Physics and Controlled Fusion, Belfast, 2017*, ECA **41F**, P2.154 (2017). <http://ocs.ciemat.es/EPS2017-PAP/pdf/P2.154.pdf>.
2. D. K. Akulina, G. A. Gladkov, Y. I. Nechaev, and O. I. Fedyanin, *Plasma Phys. Rep.* **23**, 28 (1997).
3. A. I. Meshcheryakov, I. Yu. Vafin, and I. A. Grishina, *Instrum. Exp. Tech.* **61**, 842 (2018).
4. A. V. Knyazev, A. A. Letunov, and V. P. Logvinenko, *Instrum. Exp. Tech.* **47**, 230 (2004).
5. G. M. Batanov, V. D. Borzosekov, L. M. Kovrizhnykh, L. V. Kolik, E. M. Konchekov, D. V. Malakhov, A. E. Petrov, K. A. Sarksyian, N. N. Skvortsova, V. D. Stepakhin, and N. K. Kharchev, *Plasma Phys. Rep.* **39**, 444 (2013).
6. G. M. Batanov, V. D. Borzosekov, L. V. Kolik, D. V. Malakhov, A. E. Petrov, A. A. Pshenichnikov, K. A. Sarksyian, N. N. Skvortsova, and N. K. Kharchev, *Vopr. At. Nauki Tekh., Ser. Termoyad. Sintez*, No. 2, 70 (2011).
7. G. M. Batanov, V. D. Borzosekov, D. V. Malakhov, and V. D. Stepakhin, in *XLIV International Zvenigorod Conference on Plasma Physics and Controlled Fusion, Zvenigorod, 2017*, Book of Abstracts, p. 119. [http://www.fpl.gpi.ru/Zvenigorod/XLIV/Mu/en/CM-Batanov\\_e.docx](http://www.fpl.gpi.ru/Zvenigorod/XLIV/Mu/en/CM-Batanov_e.docx).
8. A. A. Pshenichnikov, L. V. Kolik, N. I. Malykh, A. E. Petrov, M. A. Tereshchenko, N. K. Kharchev, and Yu. V. Khol'nov, *Plasma Phys. Rep.* **31**, 554 (2005).

<sup>1</sup> At present, the authors cannot assert with absolute confidence what causes these Doppler shifts: whether it is due to the poloidal rotation of the plasma as a whole or the poloidal phase velocities of the density fluctuations from which radiation is scattered.



9. V. V. Alikae, A. A. Bagdasarov, N. L. Vasin, V. A. Vershkov, S. A. Grashin, D. L. Rudakov, A. V. Sushkov, A. V. Chankin, and V. V. Chistyakov, in *Proceedings of the 17th EPS Conference on Controlled Fusion and Plasma Heating, Amsterdam, 1990*, ECA **14B**, 1076 (1990).
10. K. Lackner, O. Gruber, F. Wagner, G. Becker, M. Besenrodt-Weberpals, B. Bomba, H.-S. Bosch, H. Bruhns, R. Buchse, A. Carlson, G. Dodel, A. Eberhagen, H.-U. Fahrbach, G. Fussmann, O. Gehre, et al., *Plasma Phys. Controlled Fusion* **31**, 1629 (1989).
11. G. M. Batanov, V. D. Borzosekov, L. V. Kolik, E. M. Konchekov, D. V. Malakhov, A. E. Petrov, K. A. Sarksyian, V. D. Stepakhin, and N. K. Kharchev, *Plasma Phys. Rep.* **43**, 1052 (2017).
12. G. M. Batanov, V. D. Borzenkov, E. M. Konchenkov, D. V. Malakhov, K. A. Sarksyian, V. D. Stepakhin, and N. K. Kharchev, *Inzh. Fiz.*, No. 10, 56 (2013).
13. E. V. Suvorov and A. A. Fraiman, *Sov. J. Plasma Phys.* **6**, 639 (1980).
14. A. S. Sakharov, *J. Phys. Conf. Ser.* **1094**, 012011 (2018).
15. E. Z. Gusakov and A. Yu. Popov, *Nucl. Fusion* **51**, 073028 (2011).
16. K. Itoh, S. I. Itoh, and A. Fukuyama, *J. Phys. Soc. Jpn.* **58**, 482 (1989).
17. U. Stroth, T. Geist, J. P. T. Koponen, H.-J. Hartfuß, P. Zeiler, and ECRH and W7-AS team, *Phys. Rev. Lett.* **82**, 928 (1999).
18. V. Erckmann and U. Gasparino, *Plasma Phys. Controlled Fusion* **36**, 1869 (1994).
19. V. F. Andreev, A. A. Borschegovskij, V. V. Chistyakov, Yu. N. Dnestrovskij, E. P. Gorbunov, N. V. Kasyanova, S. E. Lysenko, A. V. Melnikov, T. B. Myalton, I. N. Roy, D. S. Sergeev, and V. N. Zenin, *Plasma Phys. Controlled Fusion* **58**, 055008 (2016).
20. S. Wang, H. Liu, Y. Jie, Q. Zang, B. Lyu, T. Zhang, L. Zeng, N. Zhang, N. Shi, T. Lan, Z. Zou, W. Li, Y. Yao, X. Wei, H. Lian, et al., *Plasma Sci. Technol.* **19**, 015102 (2017).
21. X. Wang, S. Mordijck, E. J. Doyle, T. L. Rhodes, L. Zeng, G. R. McKee, M. E. Austin, O. Meneghini, G. M. Staebler, and S. P. Smith, *Nucl. Fusion* **57**, 116046 (2017).
22. V. A. Vershkov, D. A. Shelukhin, G. F. Subbotin, Yu. N. Dnestrovskij, A. V. Danilov, A. V. Melnikov, L. G. Eliseev, S. G. Maltsev, E. P. Gorbunov, D. S. Sergeev, S. V. Krylov, T. B. Myalton, D. V. Ryzhakov, V. M. Trukhin, V. V. Chistiakov, et al., *Nucl. Fusion* **55**, 063014 (2015).
23. T. S. Hahm and P. H. Diamond, *J. Korean Phys. Soc.* **73**, 747 (2018).  
<https://doi.org/10.3938/jkps.73.747>

*Translated by I. Grishina*